Multifunctional electromechanical and thermoelectric (poly(ethylene-vinyl acetate) latex composites for wearable devices

Laura Horta Romaris[1], M. Victoria González Rodríguez[1], Bincheng Huang[2], P. Costa[3,4], Aurora Lasagabáster Latorre[1,5], Francisco Rivadulla Fernández[6], S. Lanceros-Mendez[7,8], María José Abad López[1]

[1] Grupo de Polímeros, Centro de Investigacións Tecnolóxicas, Universidade da Coruña, Campus de Ferrol, 15471 Ferrol, Spain. mjabad@udc.es

[2] Dpt of Automobile Engineering, School of Transportation Science and Engineering, Beihang University, Beijing, 100191, China

[3] Centre of Physics, University of Minho, 4710-057 Braga, Portugal

[4] Institute for Polymers and Composites IPC/I3N, University of Minho, 4800-058 Guimarães, Portugal

[5] Dpto Química Orgánica I, Facultad de Óptica, Universidad Complutense de Madrid, Arcos de Jalón 118, 28037Madrid, Spain.

[6] Centro de Investigación en Química Biológica y Materiales Moleculares, Jenaro de la Fuente s/n, Campus Sur, Universidad de Santiago de Compostela, 15782-Santiago de Compostela, Spain

[7] BCMaterials, Basque Center Centre for Materials, Applications and Nanostructures, UPV/EHU Science Park, 48940 Leioa, Spain

[8] IKERBASQUE, Basque Foundation for Science, 48013 Bilbao, Spain

Graphical Abstract

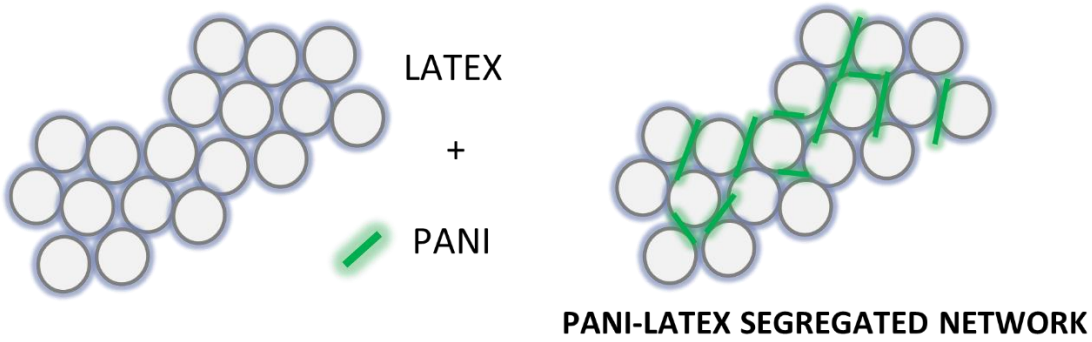

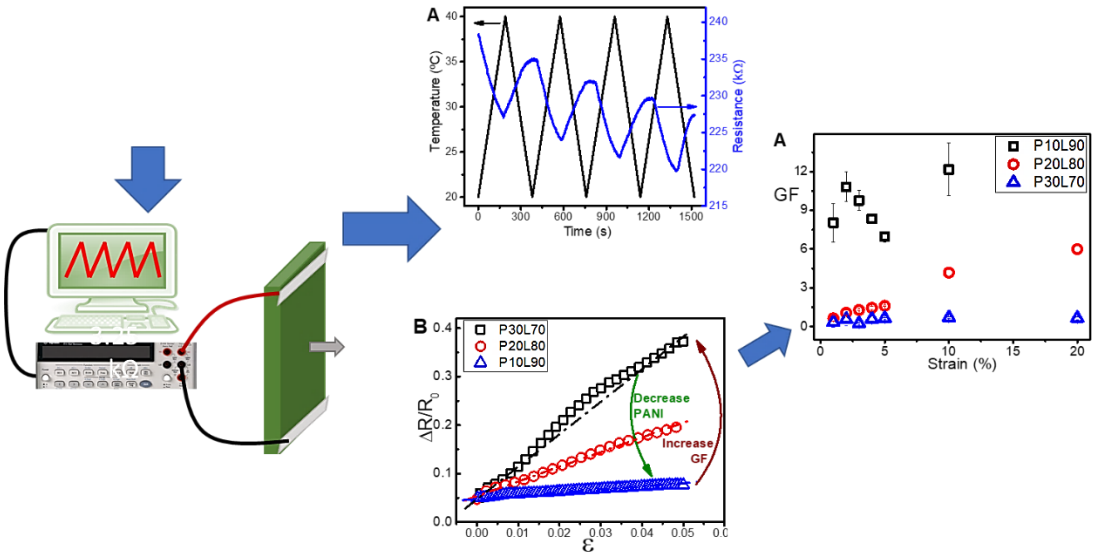

Abstract

This paper reports on the piezoresistive, thermoresistive and thermoelectric behaviour of polymer-based nanocomposites, composed of polyaniline and poly(vinylacetate) latex (PANI/PVAc) matrix. The samples were prepared by simple, scalable, eco-friendly and low-cost latex technology with PANI concentrations spanning form 2.5 to loadings of 60 wt.%.

The observed electrical and mechanical behaviour can be explained in the framework of the percolation theory. Specifically, stretchable PANI/PVA_c films with PANI contents ranging from 10 to 30 wt.% are particularly useful for applications involving electrical conductivity with elastomeric performance. Due to the combination of the reinforcement effect of PANI and enhanced interfacial adhesion via H-bonding between PANI and the polymer matrix, they present higher Young´s modulus and tensile strength together with a slight decrease in ductility, compared to pure PVAc latex.

PANI/PVA_c ratio plays an important role in the electromechanical composites, both in the GF values and fatigue. Accordingly, the mechanical properties of PVA_c latex, tailored with conductive PANI, can develop interesting electromechanical properties for sensors devices up to large deformations. This tunability together with the soft nature of composites paves the way for low-cost macroscale diverse and adaptable applications such as temperature sensing, mapping, and compensation in stretchable and wearable electronics.

Key words: Conducting polymers; Nanocomposites; Polyaniline Blending; Thermoelectric; Piezoresistive polymers

1. Introduction

Recently, there has been remarkable accomplishment in the field of stretchable electronics including display panels, radio frequency electronics, light emitting diodes, acoustic devices, elastic conductors, smart sensors, artificial muscles, electronic skin health monitoring systems and other wearable devices [1–4]. Excellent mechanical properties combined with thermoelectric performance, piezoresistive and thermoresistive properties are among the capabilities required for components used in the fabrication of integrated stretchable systems for the aforementioned applications.

The rapid development of next-generation stretchable electronics stimulates the urgent demand for novel, low-cost, ecofriendly, simple processing, light weight and flexible materials. Intrinsically conductive polymers (ICP) such as polyaniline (PANI), poly(3,4-ethylenedioxythiophene) (PEDOT), PEDOT modified with polystyrenesulfonate acid (PEDOT/PSS) or polypyrrole (PPy) represent a fascinating class of materials that can fulfill these requirements and can be an alternative to the currently used commercial metallic and/or ceramics components, although to become competitive with present, novel materials will need to increase in efficiency [3,5–7].

PANI is the most investigated ICP both by academics and industry [5] and can be considered unique owing to its reversible doping/dedoping that affects their electrical conductivity by several orders of magnitude [8]. It has been proven that PANI doped with an inorganic acid, such as hydrochloric acid (PANI-HCl) shows suitable electrical conductivity at room temperature [9]. However, PANI-HCl presents low thermal stability [9] and its electrical conductivity suffers variations for small temperature and humidity changes [10] that can represent a disadvantage for some technological applications, which require heat molding [11]. Other drawbacks are poor mechanical properties [6] and its intractability, i.e., insolubility in common solvents and infusibility, which results in poor processability [12]. A strategy to overcome these issues is the design of novel conductive polymer composites (CPC) which combine the interesting PANI properties with the mechanical performance of insulating thermoplastic or elastomers [ref]. Thus, the new composites must be molded at room temperature in order to obtain more flexible and ductile materials than PANI.

The literature, presents several examples of PANI blending with several host matrices such as poly(n-butyl methacrylate) (PBMA) [13], poly(dimethysiloxe) (PMDS) [11], styrene-butadiene-styrene copolymer (SBS) [14,15] or poly(ethylene-vinyl acetate) (PVAc) [16] with promising piezoresistive behaviour for deformation sensors [17]. By

contrast, fewer studies have been reported about PANI composites used in the fabrication of flexible temperature sensors [2]. Besides, although the thermoelectric performance of several nanocomposites based on PANI-inorganic fillers and PANI-carbonaceous materials has been widely studied, [3,18–20], to date, there are no reports describing the thermoelectric properties of PANI/thermoplastic elastomer blends. At any rate, tailoring polymeric blends with specific thermal and electrical properties for smart materials is an interesting scientific and industrial alternative for the actual sensors market.

In this context, this paper deals with the development of polyaniline/ poly(ethylene-vinyl acetate) latex nanocomposites (PANI/PVAc) obtained by film–casting at room temperature. Latex technology, which uses water-based polymer emulsions, favors the retention of conductive fillers within the interstitial space between the latex particles upon water evaporation and, thus, the formation of a segregated CPC (s-CPC). This is a low cost and environmentally friendly approach to obtain flexible CPCs with excellent electrical properties, as it does not require the use of toxic and inflammable solvents [21–23].

Composites with PANI contents between 10 and 30 wt.% combine suitable electrical conductivities and the beneficial mechanical properties of the polymer matrix with hardly decreasing the polymer matrix thermostability. The thermoelectrical, electromechanical behaviour and thermoresistive properties of selected composite films are evaluated in order to elucidate the viability of these materials for large deformations sensors, thermal sensors or other softstretchable electronic applications. Composite films with PANI contents slightly above the percolation threshold resulted to be more sensitive to mechanical deformation and thermal stimulus that those of particle contents far above the percolation threshold. By contrast, the latter exhibit higher electrical conductivity, thermoelectric performance and fatigue resistance.

2. Experimental details

2.1. Materials

Aniline and potassium peroxodisulfate (APS) were purchased from Fluka (Steinheim, Germany). Concentrated HCl acid was obtained from Scharlau (Sentmenat, Spain). All the solvents and reagents were at least of 99% purity and used without further purification. Water was purified on a Milli-QUltrapure 109 system (Millipore, Molsheim, France).

Polyaniline doped with hydrochloric acid (PANI-HCl), prepared as described by Park [24], filtered under vacuum and freeze-dried has an estimated molecular weight of 6,300

g/mol. Vinnapas EP 4014 latex, supplied by Wacker (München, Germany), is an aqueous, plasticizer-free polymer dispersion of poly(ethylene-vinyl acetate) (PVAc) (55 wt.% solids in water). The experimental determined amount of vinyl acetate comonomer from elemental analysis (EA) is 72.4.% The densities of PVA_c and PANI-HCl, calculated by the Archimedes method, are 1.039 and 1.26 $g.cm^{-3}$, respectively.

2.2.Composite preparation

A simple cast film method was followed for the preparation of PANI/PVAc latex composites, preceded by the physical mixture of the components. A prerequisite for the successful implementation of latex technology is the stable dispersion of nanofillers in water [23]. Therefore, after homogenizing PANI powder in a mortar, water was added and the resulting solution was sonicated during 5 min using a Digital Sonifier 450, Branson. The aqueous PANI dispersion was then combined with Vinnapas latex and sonicated between 5-30 min depending on the composition. Finally, this mixture was cast on a teflon mold as a film and the solvent was allowed to evaporate for 72 h at room temperature. The resultant dry films have an opaque black appearance with thicknesses ranging from 150 to 300 μm (MarCator 1080, Mahr digital micrometer). The nomenclature adopted for the PANI/PVAc latex composites, the composition and the mechanical behavior of the films are shown in Table 1.

Table. 1. Composition of PANI/PVAc composites.

Composites	***PANI (wt.%)***	***PANI (vol.%)****	***Type of film***
L100	-		Ductile
P2.5L97.5	2.5	2.1	Ductile
P5L95	5	4.2	Ductile
P10L90	10	8.4	Ductile
P17L86	17	15	Ductile
P20L80	21	18	Ductile
P30L70	27	23	Ductile
P34L66	34	30	Ductile
P41L59	41	36	Less Ductile
P43L57	43	38	Less ductile
P46L54	46	41	Brittle

P50L50	50	45	Very Brittle
P55L45	55	50	Very Brittle

* The volume additivity law is used to convert weight% to volume%.

2.3. Composite characterization

The morphology of the composites was evaluated by transmission electron microscopy (TEM) with JEOL JEM 1010 (80 KeV) equipment after applying 10 μL of the aqueous pre-composites dispersions to a cupper grid.

Tapping mode atomic force microscopy (AFM) is used to characterize film topography of a representative composite; measurements at room temperature were performed using a commercial Veeco-Brucker MultiMode system. The system is combined with the high-sensitivity conductive working mode (C-AFM) that allows imaging morphology along with local current. The stylus of the C-AFM tip behaves as the top electrode in the microscale dimension; it is parked on the top of the polymer bump and a voltage scan is applied from 3 to -3 V while measuring the current.

The Fourier-transform infrared (FTIR) data were recorded on a Jasco 4700 spectrometer equipment. The absorption spectrum of the PANI-HCl was performed in Potassium Bromide (KBr) pellets. The PVAc and composite films were analyzed in the attenuated reflection mode (ATR-IR) by using the above mentioned spectrometer equipped with the MIRacle^{TM} ZnSe Single Reflection Horizontal ATR Accessory. All the spectra were collected from 4000 to 600 cm^{-1} with a 4 cm^{-1} resolution over 100 scans and subjected to baseline correction. The spectra of the films were further subjected to ATR correction and the intensities were normalized with respect to the maximum of the carbonyl peak ($\nu_{C=O)}$ of PVAc at 1731 cm^{-1}.

X-ray patterns of PANI powders were recorded in step-scan mode from 2º to 50º with a 2θ step of 0.05º using a D5000 diffractometer (XRD, Siemens- Bruker) with CuKα line irradiation (λ= 1.541Å). A split Gaussian function was used to subtract the background and amorphous contributions using the open-source software Fityk. The difference patterns were deconvoluted into the crystalline constituents using Gaussian function peak shape approximation [25]. The degree of crystallinity (X_c) was estimated from the percentage of crystalline peak area to total scattered area. The d-spacing was calculated using the Bragg equation and the crystallite domain size (L) was evaluated using the Debye-Scherrer formula from the full width at half-maximum (FWHM) [26].

Tensile stress–strain properties were characterized using an Instron 5566 universal testing machine (Instron Canton, MA) operating at room temperature and at a crosshead speed of 5 mm/min for 5 min, followed by a test speed of 50 mm.min^{-1} until failure. Young modulus (E) and strength and strain at break point (σ_y and ε_y) were calculated from stress-strain curves as the average of five rectangular shaped samples of 150 x 15 mm and thickness ≈0.5 mm.

Thermogravimetric analysis (TGA) was performed with a Perkin-Elmer TGA-7 over a temperature range of 25 to 800 °C at a heat rate of 10 °C/min under oxygen atmosphere.

The thermoelectric figure-of-merit (ZT) is a common measure of a material's energy conversion efficiency:

$$ZT = \frac{\sigma\alpha^2}{\kappa}T \quad (1)$$

Where σ, α, κ, and T are electrical conductivity, Seebeck coefficient, thermal conductivity and absolute temperature, respectively [19]. The three parameters constituting ZT were measured on the PANI/ PVAc latex films.

Electrical resistivity at room temperature was calculated by the four-point method (LORESTA-GP, Mitsubishi Chemical, MCP-T610). The electrical conductivities (σ) reported for each polymer are the mean values of at least 40 readings determined on different samples. Conductivity was measured on the top and bottom surfaces to confirm homogeneity of PANI/PVAc films.

The Seebeck coefficient (α) was measured using a home-made device depicted in Fig. S1 (Supporting information). The sample was mounted between two copper blocks (4 x 4 mm^2), while a heat pulse was applied to one end of the sample to create a thermal gradient. The total temperature difference was maintained below 2K, and the linear ΔV/ΔT variation was recorded at each base temperature (Fig. S2, Supporting information). The measurements were performed under vacuum between 200 and 325 K.

Thermal diffusivities were measured by the flash diffusivity technique with the thermal analyzer (LFA 447 Nanoflash, Germany) on square samples of 8 x 0.5 mm of length and thickness, respectively, at 300 K. Test samples were sprayed with a coating of graphite on both sides before testing. Pulse corrected Cape Leman model was used to analyze the data in analysis software. The thermal conductivities were derived from the following equation:

$$\kappa = a\,\rho\,c_p \quad (2)$$

Where κ is the thermal conductivity, a is the thermal diffusivity, ρ is the density of samples and c_p is the specific heat capacity. The density has been estimated from the additivity law. The specific heat capacity c_p was obtained by Differential Scanning Calorimetry (DSC TA Instruments 2010) using sapphire as reference material and following the standard UNE-EN ISO 11357-4[27].Both thermal diffusivity and specific heat capacity are the average value of three replicas for each sample.

Electromechanical measurements were carried out using the universal testing machine (Shimadzu AG-IS) in uniaxial strain mode. Rectangular samples of 20 x 10 mm and thickness of ≈0.5 mm were analyzed. The silver painted electrodes were placed inside the mechanical claws for good electrical contact and for avoiding any deformation during mechanical cycles. The electromechanical behaviour of the PANI/PVAc composites was evaluated as the average of 4 uniaxial load-unload cycles at 1, 5 and 10 mmmin^{-1} for 1, 2, 3, 4, 5, 10 and 20% of deformation (Fig. 1). The electrical resistivity variation was evaluated with a digital multimeter (Agilent 34401A). In order to analyze the long time electromechanical stability, 100 cycles were performed for 5% deformation at 5 mm/min. All experiments were conducted in atmosphere at room temperature.

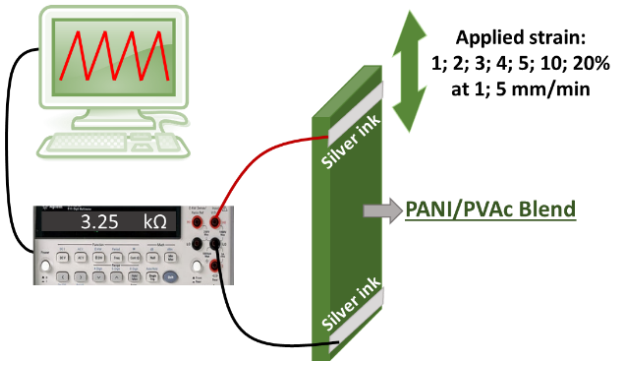

Figure 1. Electromechanical analysis of the PANI/PVAc composite films from low to larger strains. The deformation was varied from 1 to 20% at 1, 5 and 10 mm.min^{-1}.

The electromechanical sensibility of the blends was evaluated by the gauge factor (GF) defined as [28]:

$$GF = \frac{\Delta R/R_0}{\Delta l/l_0} = \frac{d\rho/\rho_0}{\varepsilon} + 1 + 2\nu \qquad (3)$$

where R is electrical resistance, v is Poisson coefficient, l the mechanical displacement and $\varepsilon = \Delta l / l_0$. The geometrical factor $(1 + 2v)$ depends on the properties of the materials where the maximum value is $GF \approx 2$ for elastomers with a Poisson coefficient of 0.5 [29]. The thermal effect on the resistive properties of the blends was measured using a digital multimeter Agilent 34401A (for measuring the electrical resistance) synchronized in real time with the temperature oven Linkam THMSE 600. The temperature changes from 20 up to 40 ºC and from 20 up to 100 ºC at a rate of 10 ºC.min^{-1}.

3. Main results and discussion

3.1. Morphological and structural characterization

The morphology of PANI nanoparticles and PVAc latex micro-spheres in the initial dispersion was determined by TEM analyses. Figure 2A shows that pure PVA_C latex consists of spherical particles with diameters between 0.5 and 1 µm. In *P30L70* dispersions (Fi. 2B-C), PANI-HCl exhibits the same nanorod morphology described in a previous work [30]. Nanorods with 10-15 nm diameter and variable length from70 to 300 nm, are highly aggregated forming small clusters of thickness ranging from 65 to 95 nm.

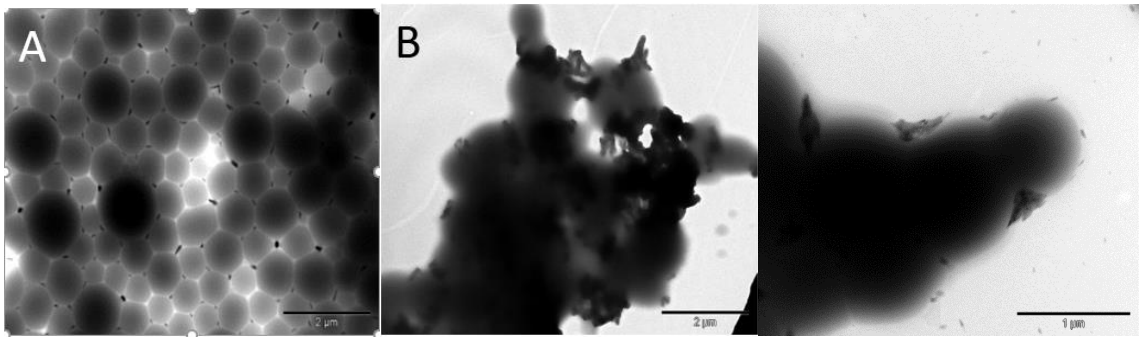

Figure 2. TEM images of A) PVAc latex film and B) *P30L70* dispersion at x15 000 magnification and C) *P30L70* x40 000 magnification.

Smaller agglomerates or individual nanorods, will eventually fill the interstitial space between the latex µspheres and creates the interconnected conductive pathways, as is confirmed by AFM images (in Fig. 3).

AFM in conductive mode is used to image the conducting PANI network inside the blends. Composites with PANI contents below 30 wt.% are too resistive to be measured

by this technique; therefore, the surface morphology of the composite *P30L70* was scanned (Fig. 3 A) and then, the conductive tip was parked on the top of the bump and a voltage scan applied (Fig. 3. C). The 30 x 30 μm three-dimensional and height images provide a detailed view of the particle arrangement and a unique insight of the distribution of the conductive phase within the matrix.

Conductive PANI is organized around oval domains of PVA_c latex and confined in the small voids observed at the junction of latex particles, forming a segregated conductive network throughout the observed area, with the inevitable presence of randomly distributed aggregates forming microvoids. Besides, the film topography is dominated by a softly undulating smooth surface but with the boundaries of the individual PVA_c particles still visible at the surface. The original spherical particles deform, forming large boulder-like bumps, but polymer interdiffusion is not sufficient to make the inter-particle boundaries disappear due to the low drying temperature [31].

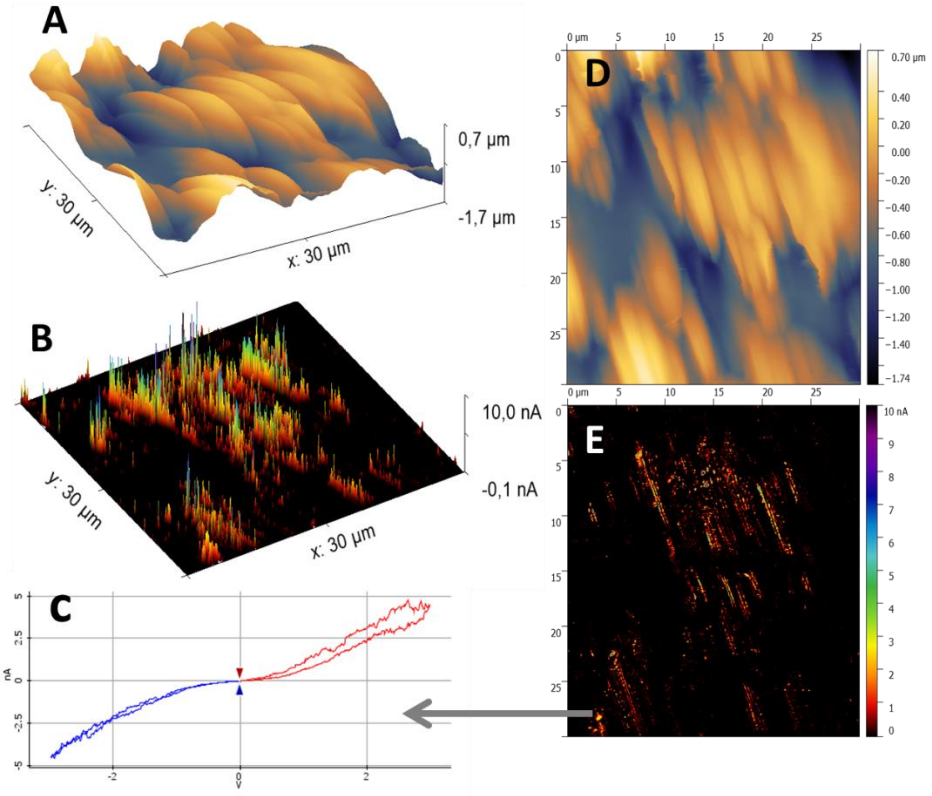

Figure 3. AFM micrographs of *P30L70* obtained with a conductive tip. Two types of distinct surface structures 3D (A and B) and 2D (D and E) respectively for: A) topography B) electrical current intensity. C) Example of the C-AFM measurement.

Additionally, ATR-FTIR spectroscopy of PANI/PVAc composites provides evidence of interaction between the two components. Figure 4 shows the FTIR spectra of virgin PANI-HCl and PVAc films (thoroughly described in Supporting Information, S2.1) compared to the spectrum of a representative composite film, *P30L70*.

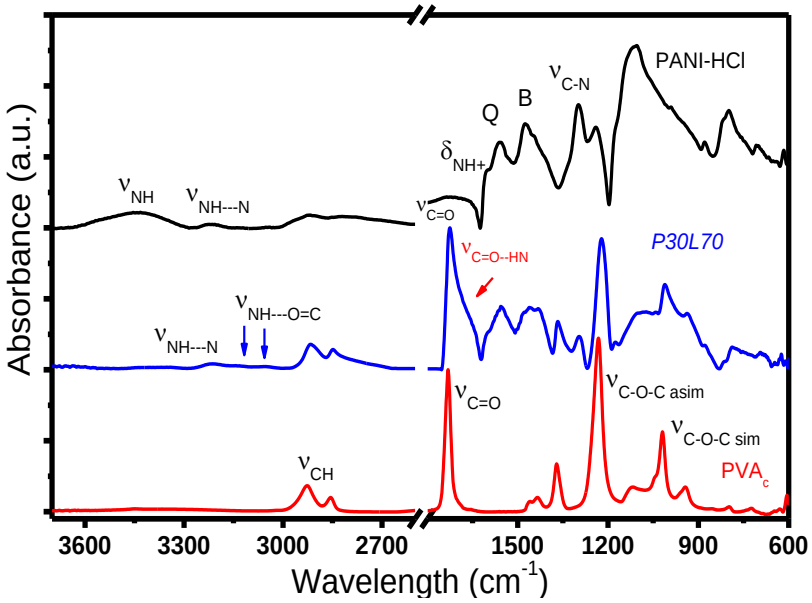

Figure 4. FTIR spectra of PANI-HCl, polyvinyl acetate (PVAc) latex and the composite film *P30L70*, between 600 and 3700 cm^{-1}..

In all the composites spectra characteristic peaks (data not shown) of both components can be perceived, together with the enhancement of the intensity of PANI peaks upon increasing PANI loading. Further, some peaks shift and the appearance of new bands are indicative of interaction between both polymers. Specifically, the PANI peaks at 3432 and 3220 cm^{-1} (ν_{NH}) downshift to 3300 and 3200 cm^{-1}, respectively, and two new peaks appear at lower wave numbers, 3130 and 3049 cm^{-1}, as a result of hydrogen bonding (H-bonding) with PVAc acetate groups.

Concerning PVAc, the absorption maximum of the carbonyl stretching band ($\nu_{C=O}$) at 1731 cm^{-1} linearly downshifts with increasing PANI loading, reaching the value of 1720 cm^{-1} for composites with high PANI contents. Concurrently, the band broadens due to the gradual development of a shoulder at 1715 cm^{-1}, which is assigned to vibrations of bound carbonyl groups ($\nu_{C=O--HN}$) (Fig. S3A, Supporting information) [32,33]. The carbonyl band is used to characterize the fraction of H-bonded carbonyl groups (f_b) by analyzing the vibrations of free ($\nu_{C=O}$) and bound ($\nu_{C=O--HN}$) carbonyl groups, as described in Supporting information (Fig. S3B, Eq.S1, Supporting information). f_b is plotted versus

PANI weight percentage in Fig. 5. The PVA_c bound fraction exponentially increases with the raise of PANI weight (R^2=0.94), reaching a constant value of 0.45 for PANI contents ≥30 wt.%.

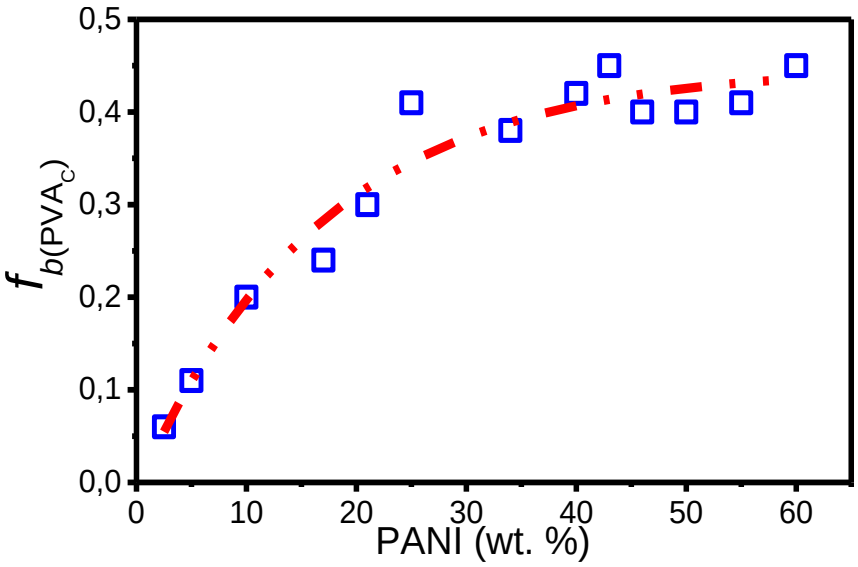

Figure 5. Fraction of bound carbonyl groups (f_b) of PVA_c versus wt.% PANI from a fit of two Gaussian bands to the carbonyl region of the ATR spectra. The dashed line is an exponential fit to the data.

Taking into account the above results, H-bonding can be analyzed from the point of view of PANI chains hereafter. The PANI structural formula has four potential NH donor groups, whereas PVAc structural formula has 1 only carbonyl acceptor group. The data of Fig. 5 mean that, on average, ≈4 NH groups of the PANI structural formula are involved in H-bonding for 5 wt.% PANI; ~2 NH groups for 10 wt.% PANI; ~1 NH group for 21 wt.% PANI and less than 1 NH group for PANI contents ≥30 wt.%.

Additionally, the upshifts of several PANI bands (δ_{NH}^{+}, Q, B), which are indicative of the protonation level [34], suggest a partial deprotonation of PANI-HCl for PANI contents below 30 wt.% (Fig. S4, Supporting information). On increasing PANI loading, these bands maxima gradually downshift, reaching values similar or lower than those of pristine PANI-HCl. These results may be explained by the strong H-bond interaction between PANI and PVAc which, as stated in the preceding paragraph, encompass more NH groups of the PANI structural formula at low PANI contents than at higher concentrations, thus promoting a partial deprotonation in the former compositions.

XRD analysis confirms the strong dependence of the composites morphology on the PANI content (Fig. 6). The PVAc film displays the typical behavior of an amorphous polymer, while neat PANI-HCl exhibits partial crystallinity, indicative of the orthorhombic structure of ES-I type, with the most intense reflection at 2θ = 25.6° [26]. In turn, the XRD patterns of the PANI-PVAc composites contain the characteristic features of the scattering of both polymers for PANI contents above 20 wt.%; beyond this value, the crystallinity fraction of PANI within the composite has been estimated (Table S1, Supporting information). Both the crystallinity fraction and the intensity of the peak at 2θ =25.6° linearly increase with increasing the PANI weight fraction, approaching the value of pure PANI-HCl. No peaks shifts have been observed, but the narrowing of the peak at 2θ =25.6° reflects an increase in the size of the crystals. In short, the lower crystallinity of the PANI fraction at low filler contents may be enhanced by the partial PANI deprotonation observed by FTIR.

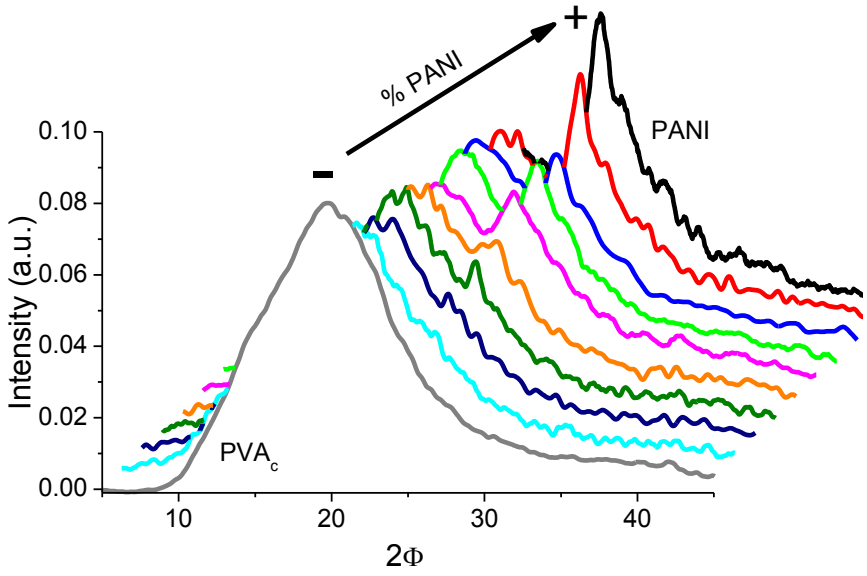

Figure 6. X-ray diffraction patterns of PVAc film to neat PANI, and PANI-PVAc composites of increasing PANI content (between both materials).

3.2. Electrical properties

The room temperature electrical conductivities of PANI/PVAc composites, which were identical on both sides, increase from 10^{-7} to 4 S.cm^{-1} as a function of the PANI volume percentage (Fig. 7, green circles). Following the percolation theory, the lowest filler concentration for a composite with an insulating matrix to become conductive, corresponds to the so-called percolation threshold (ρ_c). At this limit concentration, a

sharp increase in conductivity of several orders of magnitude occurs. For the mathematical determination of ρ_c, the data are fitted to the corresponding power law (inset Fig. 7) [35,36]. The experimentally estimated percolation threshold (ρ_c) is ~7.5 vol.%, the effective conductivity of PANI-HCl within the matrix (σ_0) is ~ 2 S/cm and the critical exponent *t* is 2.86; the latter value indicates that the conduction in this composite occurs in 3D [36].

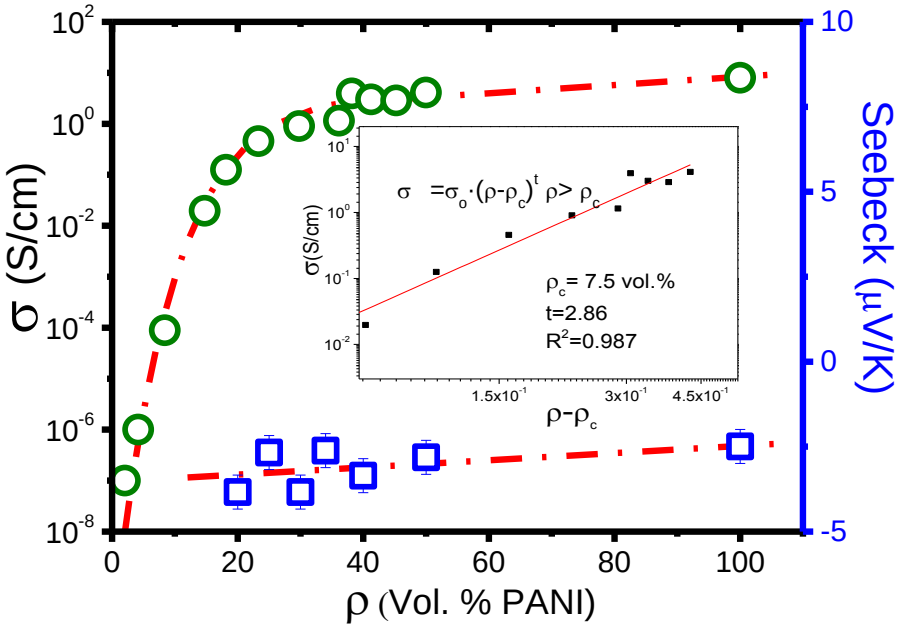

Figure 7. Electrical conductivity (in semi-log plot, green circles) and Seebeck coefficient (blue squares) as a function of vol% PANI (ρ). The insert shows a log–log plot of the conductivity as a function of ρ−ρc.

The percolation thresholds (ρ_c) of different PANI-polymer composites prepared by film casting varied from 3 to 10 vol.% [13,37,38]. By contrast, a very low ρ_c of 0.60 vol.% has been obtained by Levin et al. for a PANI/PVAc segregated network; nonetheless, the geometry and molecular weight of PANI nanoparticles used by these authors are different than ours and the highest electrical conductivity values achieved are two orders of magnitude lower [16]. These discrepancies are not surprising since the values of ρ_c and maximum electrical conductivity reached by different CPCs are strongly dependent on the nature of the fillers, their aspect ratio and shape, filler dispersion, elastomer matrix and filler distribution in the nanocomposite [21].

In the current experiment, the strong H-bond interaction between PANI and the polymer matrix promotes a partial deprotonation of PANI and a lower crystallinity degree at low filler contents. These structural features may account for the obtained percolation threshold. Most importantly, the electrical conductivities of composites with PANI contents above 30 wt.% are similar to pristine PANI-HCl.

3.3.Thermoelectric properties

The potential of PANI/PVAc composites as organic thermoelectric materials has been investigated. Despite the significant increase in electrical conductivity, the Seebeck coefficient (α) values of the PANI/PVAc composites are similar to pure PANI-HCl (-2.5 μV/K), within experimental error (Fig. 7, squares). Likewise, the thermal conductivities (κ) (0.4-0.5 W/m·K) are independent of the filler concentration for PANI contents below 40 wt.%, although they are twofold the value of pure PANI (0.22 W/m·K). According to previous authors and opposite to bulk semiconductors, in the case of polymer composites it is easy to enhance electrical conductivity keeping α and κ constant on increasing the filler amount [20,39]. This feature is ideal for tailoring thermoelectric properties and has been explained by the thermally disconnected, but electrically connected, junctions in the segregated conductive networks [39].

Following eq. 1, ZT values are calculated using the three described parameters, σ, α and κ, at room temperature. ZT increases from $1.2\cdot10^{-7}$ to $1.2\cdot10^{-6}$ for PANI contents spanning from 25 to 50 wt.%. Specifically, the ZT values of *P20L80* and *P30L70* are 1.2×10^{-7} and $3.7\cdot10^{-7}$, respectively; the latter is an order of magnitude lower than the ZT of pristine PANI-HCl ($3.4\cdot10^{-6}$). Even though the experimental ZT is still low for commercial applications, the results are promising since these lightweight stretchable composites are ecofriendly, low cost and easily scalable for industrial implementation without dimensional limitations. Apart from ZT, the global efficiency of a thermoelectric device depends on the thermodynamic efficiency and device design. In these sense, PANI/PVAc composites display higher versatility than nanocomposites based on PANI/ semiconducting inorganic particles, therefore widening potential applications, specifically in large are applications [19].

3.4.Mechanical properties

The influence of PANI on the mechanical properties of PVA_c based composites was studied by tensile testing for three formulations above the percolation threshold, *P10L90, P20P80 and P30L70. A*t PANI loadings larger than 40 wt.% the composite films become brittle, probably due to the fragile behaviour of filler particles and their agglomerates. The Young modulus (E), the stress (σ) and strain (ε) at the break point were measured from the stress–strain curves (Fig. S5, Supporting information) and the results are summarized in Table 2.

Table 2. Summary of the experimental parameters of mechanical properties.

Samples	***E* (MPa)***	**Σ (MPa)****	***E* (%)****
L100	0.85 ± 0.07	1.5 ± 0.3	492 ± 67
P10L90	2.5 ± 0.2	2.7 ± 0.1	517 ± 93
P20L80	5.6 ± 0.8	2.5 ± 0.7	302 ± 173
P30L70	12 ± 2	3.4 ± 0.2	330 ± 78

* measured at 5 $mm.min^{-1}$. ** measured at 50 $mm.min^{-1}$.

Upon increasing PANI content, the composites exhibit an increase in stiffness and tensile strength compared to pure PVAc latex films. The enhancement of Young´s modulus is expected due to the presence of rigid benzene rings in PANI chains ($E_{PANI} \approx 1.5\text{-}2.2$ GPa and $\varepsilon_{PANI} \approx 5\text{-}10\%$) [40,41]. In addition, the strong H-bond interaction, described in morphological characterization section, enhance interfacial adhesion between the PANI network and PVA_c matrix, improving the tensile strength, specifically the Young modulus and maximum strain. The maximum stress decreases for composites with 20 wt.% or higher PANI contents.

Concerning ductility, the deformation at break point of the three composites suffers a slight reduction with respect to pure latex, within the experimental error. More to the point, the relative error increases as a function of PANI content; this result indicates that the composites heterogeneity augments with higher filler amounts, owing to the agglomeration of PANI particles. Furthermore, the three composites assayed have broken without plastic deformation, confirming retention of the elastomeric nature. They all show an acceptable behavior for their use as stretching electrically conductive elastomers. These results are encouraging, as enhancing the tensile strength and ductility of s-CPC

remains a challenge and, so far, few researchers have successfully improved these properties [23].

More importantly, stretching an electrically conductive elastomer nanocomposite often results in increased electrical resistance, owing to the permanent breakdown of the filler network. Hence, the electrical conductivity was measured before and after mechanical stretching. It decreases two orders of magnitude, to half the original value and one order of magnitude for *P10L90*, *P20L80* and *P30L70* films, respectively (Fig S6, Supporting information). This fact is very relevant for the electro-mechanical properties and sensor applications [21].

3.5.Thermal stability

The effect of PANI-HCl on the thermostability of the composites is appreciated by the change of position of the main weight losses in the TGA and DTG curves (Fig. S7, Supporting information). PANI-HCl shows three main weight loss stages in the temperature ranges 40-155, 155-318 and 318-700 ºC, assigned to release of moisture and volatile components, to partial loss of HCl acting as dopant and to the loss of bound HCl from deep inside the bulk of the PANI clusters, followed by degradation of PANI chains, respectively [30]. By contrast, PVA_c latex is thermally stable up to 250 ºC. The thermal degradation occurs in three steps ranging 250-470, 470-537 and 537-615 ºC corresponding deacetylation, chain scission reactions of deacetylated vinyl acetate entities and ethylene units, respectively [42].

The relative thermal stability of the PANI/PVA_c films is evaluated by comparing decomposition temperatures at various percentage weight losses, which are presented in Table 3. The composites exhibit shifts of the moisture and HCl evaporation of the PANI phase to higher temperatures, with reduction of weight losses, as compared with those of neat PANI-HCl: on the contrary, the deacetylation step of the PVAc moves to lower temperatures, compared with that of pure PVA_c latex, owing both to the increase in moisture and HCl contents and to the catalytic effect of HCl acid on the deacetylation of PVAc [43]. At any rate, the thermostability decrease is negligible for PANI contents ≤ 10 wt.%.

Table 3. Characteristic degradation temperatures of PANI-HCl, PVA_c and PANI-PVA_c composites taken from the minima of DTG curves.

Sample	$T_{moisture}$ (weight loss)	T_{HCl} (weight loss)	T_{10}	$T_{deacetylation}$
PANI	87 (5.2%)	235 (7.2%)	263	-
LATEX	-	-	365	395
P10L90	132 (1.6%)	246 (1.6%)	364	395
P20L80	138.5 (2.8%)	237 (2.8%)	354	392
P30L70	117.0 (3.2%)	240 (3.7%)	341	387
P40L60	92.0 (3.0%)	235 (2.7%)	344	388
P50L50	83 (5.04%)	235 (3.35%)	330	377

3.6. Electromechanical response

The PANI-PVA_c composites present piezoresistive properties for PANI contents up to 30 wt.%. The piezoresistive response was analysed for *P10L90, P20L80* and *P30L70.* They all follow the typical behaviour; the electrical resistance increases while the film is stretched and decreases when the composite recovers to the initial deformation [44]. As an example, Fig. 8A depicts the electromechanical performance of a *P20L80* film for 5% of deformation at 5 $mm.min^{-1}$. Besides, the three formulations display excellent linear behaviour between mechanical stimulus and electrical resistance variation which allows GF calculation, as illustrated in Figure 8B. Additionally, the electromechanical behaviour of the three composites as a function of deformation, velocity and number of cycles is presented in Figures 9A-C.

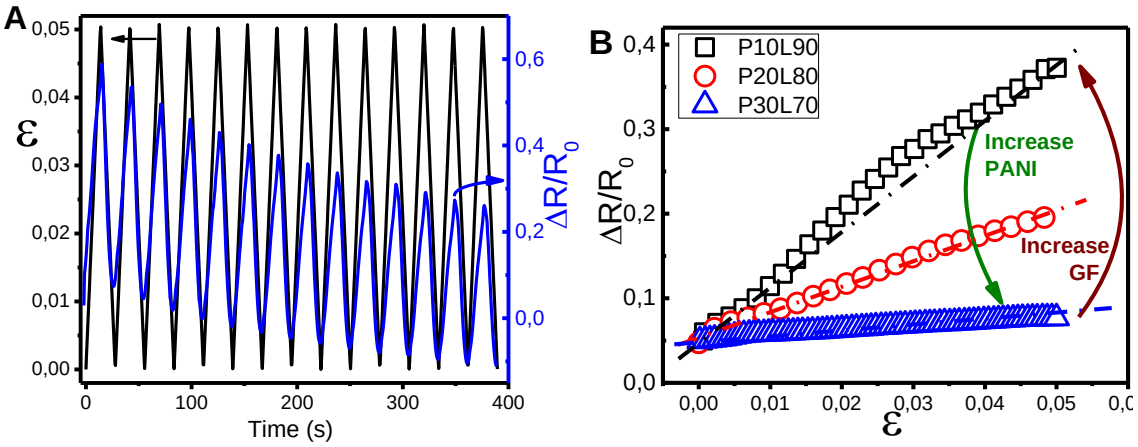

Figure 8- Illustration of electromechanical behaviour: A) Cycles for PANI20/Latex70 for 5% of deformation at 5 $mm.min^{-1}$ and B) different GF sensitivity as function of the PANI content in blends.

The electromechanical sensibility or gauge factor (GF) declines upon increasing PANI content. *P10L90*, *P20L80* and *P30L70* composites have GF ranges of 7-12, 1-6 and 0.5-1, respectively, depending on the experimental conditions (Figure 9A and B). As previously reported, the piezoresistive effect is larger near the percolation threshold, due to the tenuous connections of the conductive network that are more easily disconnected when stretched [16,45]. Accordingly, as has been observed in Figure 7, the electrical conductivity of *P10L90 i*s near the percolation threshold. On the other hand, the electrical conductivities of *P20L80* and *P30L70* lie above the electrical threshold in the curve.

This enhancement in sensitivity with decrease of PANI loadings is apparently in contrast with the results obtained by Levin et al [16] for analogous PANI-PVA_c s-CPC. The reason for this discrepancy is that all the formulations assayed by these authors are well above the percolation threshold. Quite the reverse, our results are similar to most carbon based CPC [44].

More to the point, the GF of *P30L70* is mainly determined by the geometrical piezoresistive response ($1+2\nu$) for all experimental conditions, whereas in the case of *P20L80* only for deformations less than 5% [29] (Fig. 9A-C). On the contrary, the high sensitivity of *P10L90* film is comparable to literature reports for elastomer based nanocomposites and larger than classical metal-foil strain gauges [11,16]. Besides, its piezoresistive effect is mainly influenced by an intrinsic contribution of the electrical resistance variation upon mechanical deformation.

The main conduction mechanism dominating the PANI electrical response has been ascribed both to the ability of the charge carriers to move along the polymer backbone (intra-chain mechanism) and to their ability to hop between the polymer chains (inter-chain mechanism). This second contribution becomes particularly important when the material is subjected to a force or a pressure, as in this case; hence, under strain, the space between the PANI chains increases to exceed the tunnelling distance [8].

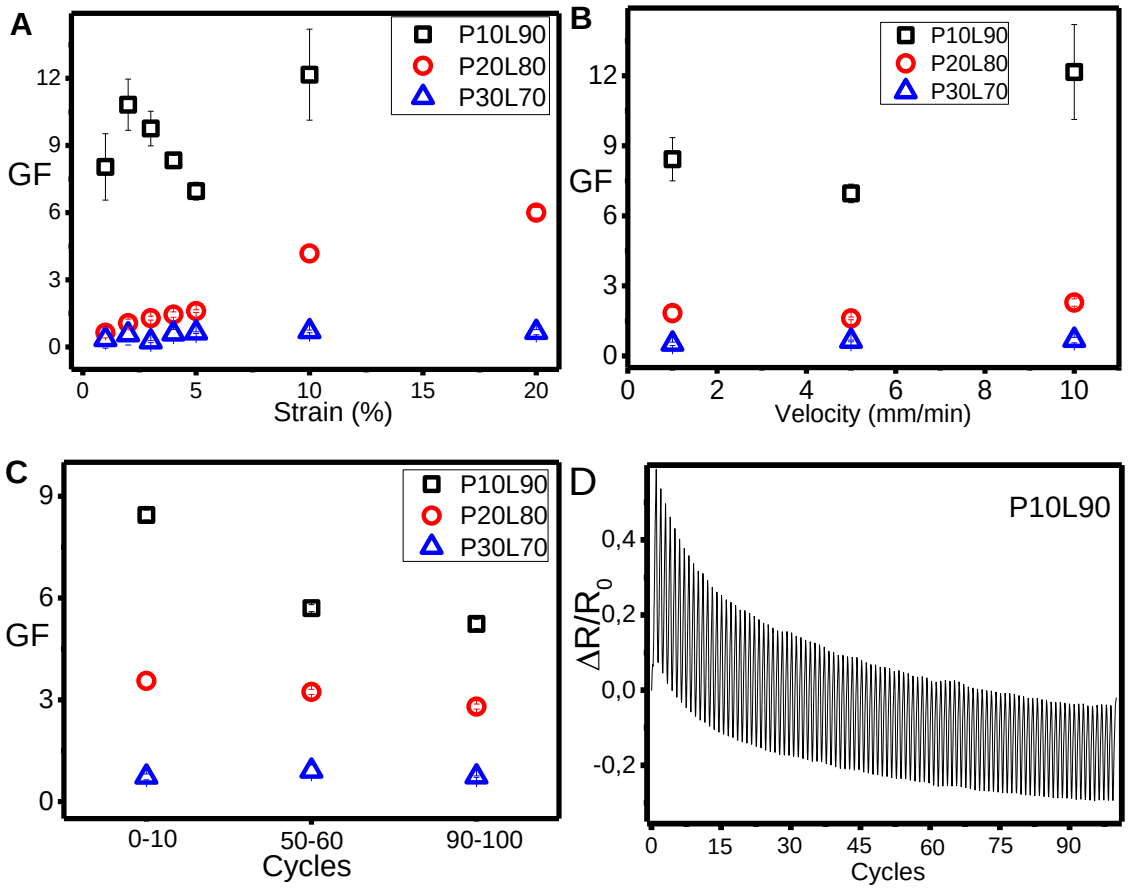

Figure 9- Piezoresistive sensitivity of PANI-PVA$_c$ composites: A) GF of *P10L90* up to 10% strain and *P20L80* and *P30L70* up to 20% strain at 5 mm/min; B) GF up to 5% of deformation at several velocities (1, 5 and 10 mm/min); C) GF as a function of the number of cycles; D) Cycle stability of the piezoresistive response of *P10L90* at 5% deformation and 5 mm/min over 100 cycles.

From another point of view, *P20L80* and *P30L70* show suitable electromechanical properties up to strains as large as 20% of deformation at several velocities; by contrast, *P10L90* only shows electromechanical response up to 10%, due to the low PANI content. Moreover, for *P10L90*, the *GF* variation with strain and velocity is erratic, but it achieves a maximum value at 10% deformation and at the highest speed of 10 mm/min (Figure 9A-B). When strain is applied, conductivity fluctuation is greater at low conductive filler concentrations due to destruction and formation of conductive paths [44].

Besides, *GF* steadily increases in *P20L80* and *P30L70* with the augment of the external stimulus, both deformation and velocity. The enhancement of the GF with strain is higher for *P20L80* than for *P30L70*. On the basis of the described conduction mechanism, the lower crystallinity degree of PANI in *P20L80* compared to *P30L70*, decreases the overall

conductivity as well as the stiffness, increasing the mobility of PANI chains and, as a consequence, leading to a larger piezoresistive response.

Finally, experiments were performed as function of the number of stretching cycles to assess the stability and fatigue of the PANI/PVA_c composites. As can be observed in Fig. 9C and D, the electrical resistance variations decrease with increasing the number of cycles in the electromechanical measurements, tending to stabilize after around 50 cycles. Nevertheless, the decline is more abrupt for *P10L90*, which decreases from ≈8 to 5 after 100 cycles and negligible for *P30L70*. Near the percolation threshold, fewer conductive channels are formed and, thus, repeated deformation-relaxation cycles result in a permanent damage to the network with possible disrupture of H-bonds between PANI and the matrix. This sensitivity loss is a common feature of thermoplastic elastomer-based CP nanocomposites [16].

3.7.Thermoresistive properties

Conductive networks within a composite film also dominate the resistance-temperature behaviour. The PANI/PVA_c composites, *P10L90, P20L80* and *P30L70*, present thermoresistive properties. The electrical resistance decreases linearly with increasing temperature and vice-versa, a clear indicator of negative temperature coefficient (NTC) behaviour. The resistivity dependence on temperature shows intrinsic semiconducting properties, which is dominated by thermally activated charge carriers [1]. The literature reports similar thermal properties for PANI-DBSA samples [30].

Besides, the thermal sensitivity of PANI/PVA_c composites declines with increasing PANI content, similarly to *GF*. This is a common behaviour as a lower carrier density is preferred to achieve higher sensitivity of NTC thermistors [1]. As an example, the results of *P10L90* films corresponding to four heating/cooling cycles from 20 to 40 °C and 20 to 100 ºC at 10 °C.min^{-1} are depicted in Fig. 10A andB, respectively. The thermoresistive sensibility is around 600 and 400 Ω/ºC for temperature variations from 20 to 40 and 20 to 100 ºC, respectively. The thermoresistive sensibility, represented by $S = \delta(\Delta R/R_0) \times {}^{100}/_{\delta T}$ [ref], is near 0.25 ±0.06 %.ºC^{-1} and 0.17 ±0.05 %.ºC^{-1} for 20 to 40 °C and 20 to 100 ºC (Figure 10 A and B, respectively).

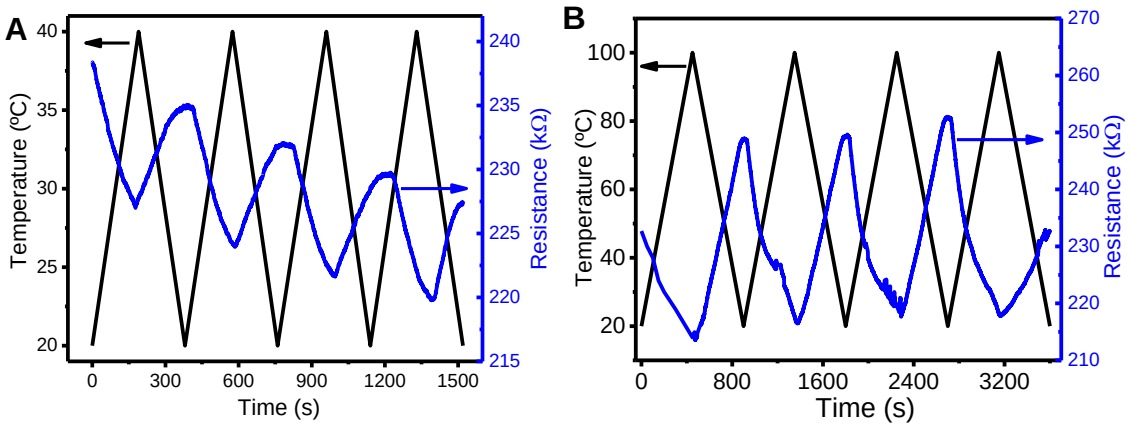

Figure 10- Thermoresistive behaviour of *P10L90* from 20 to 40 ºC A) and from 20 to 100 ºC B) at 10 ºCmin^{-1}.

Good repeatability is observed, although a drop-in resistance of ≈7 KΩ is detected at the end of the fourth cycle after heating to 40 ºC and an increase of ≈4 KΩ after heating to 100 ºC. The former observation may be due thermal doping, or to transformation of some unbound water and unbound HCl to bound forms as dopants induced by thermal energy [46]. By contrast, the latter result can be explained by the partial evaporation of moisture and volatile components (HCl) at 100 ºC, thus favouring PANI deprotonation, as described in TGA experiments.

4. Conclusions

In the current paper, the mechanical, electrical and thermal performance of PANI/PVA$_c$ composites, prepared by a easy, eco-friendly and scalable latex technology is investigated. Composite films are obtained with 3D segregated network architecture (s-CPC) and exhibit a percolation threshold (ρ_c) around 7.5% and a σ_{max} value of 4 Scm^{-1}, similar to pristine PANI-HCl. Specifically, flexible PANI/PVA$_c$ films with PANI contents ranging from 10 to 30 wt.% are particularly useful for applications involving electrical conductivity and elastomeric performance. Thermogravimetric analysis shows a small decrease in thermostability for composites with PANI contents > 10wt%.

From the point of view of thermoelectric efficiency, the composites with the maximum electrical conductivity achieve the highest ZT as the Seebeck coefficient and thermal conductivity are independent of PANI concentration. Hence, composites with PANI contents between 20 and 30 wt.% present the best compromise between thermoelectric properties and mechanical behavior.

Furthermore, the composites show satisfactory electromechanical and thermoresistive properties to be used for sensor applications. Both the Gauge factor and thermal sensitivity of PANI/PVA_c composites decline with increasing PANI content, showing the largest values near the percolation threshold. Thus, composites with 10 wt.% PANI display the highest GF, ranging between 7 and 12 for deformations spanning from 1 to 10%, similar to literature reports for elastomeric composites [47,21,11] and outperforming metal-foil strain gauges; besides, the thermal sensitivity in the temperature range 20-40 ºC is suitable for flexible and wearable temperature sensors intended for monitoring human health [4], with resistive sensibility change from 0.17 to 0.25 $\%.C^{-1}$.

By contrast, films with 20 wt.% PANI represent a reasonable compromise between response amplitude, larger deformations, and fatigue. From another point of view, electrical conductivity insensitive to deformation, as shown by composites with 30 wt.%, is important in the design of stretchable elastomer conductors [21].

In short, this study demonstrates that by adjusting the composition ratio of the PANI/PVA_c composites it is possible to tune their thermoelectric, electro-mechanical and thermal resistive properties, making them potential candidates for lightweight, stretchable electronics that could be employed as temperature and strain sensors for wearable devices.

Acknowledgments

This work was supported by the Portuguese Foundation for Science and Technology (FCT) in the framework of the Strategic Funding UID/FIS/04650/2013, project PTDC/EEI-SII/5582/2014 and grant SFRH/BPD/110914/2015 (PC). The authors acknowledge funding by the Spanish ministry of Economy and Competitiveness (MINECO) through the project MAT2016-76039-C4-3-R (AEI/FEDER, UE) and from the Basque Government Industry Department under the ELKARTEK and HAZITEK program. Bincheng Huang would like to thank the support from the China Scholarship Council.

Supplementary data

Supporting Information is available from the …… or from the author.

References

[1] C. Yan, J. Wang, P.S. Lee, Stretchable graphene thermistor with tunable thermal index, ACS Nano. 9 (2015) 2130–2137. doi:10.1021/nn507441c.

[2] S.Y. Hong, Y.H. Lee, H. Park, S.W. Jin, Y.R. Jeong, J. Yun, I. You, G. Zi, J.S. Ha, Stretchable Active Matrix Temperature Sensor Array of Polyaniline Nanofibers for Electronic Skin, Adv. Mater. 28 (2016) 930–935. doi:10.1002/adma.201504659.

[3] B. Russ, A. Glaudell, J.J. Urban, M.L. Chabinyc, R.A. Segalman, Organic thermoelectric materials for energy harvesting and temperature control, Nat. Rev. Mater. 1 (2016) 16050. doi:10.1038/natrevmats.2016.50.

[4] K. Takei, W. Honda, S. Harada, T. Arie, S. Akita, Toward flexible and wearable human-interactive health-monitoring devices, Adv. Healthc. Mater. 4 (2015) 487–500. doi:10.1002/adhm.201400546.

[5] V. Khandelwal, S.K. Sahoo, A. Kumar, G. Manik, Electrically conductive green composites based on epoxidized linseed oil and polyaniline: An insight into electrical, thermal and mechanical properties, Compos. Part B Eng. 136 (2018) 149–157. doi:10.1016/j.compositesb.2017.10.030.

[6] E. Alonso, M. Faria, F. Mohammadkazemi, M. Resnik, A. Ferreira, N. Cordeiro, Conductive bacterial cellulose-polyaniline blends: Influence of the matrix and synthesis conditions, Carbohydr. Polym. 183 (2018) 254–262. doi:10.1016/j.carbpol.2017.12.025.

[7] M. Hamid Elsheikh, D.A. Shnawah, M.F.M. Sabri, S.B.M. Said, M. Haji Hassan, M.B. Ali Bashir, M. Mohamad, A review on thermoelectric renewable energy: Principle parameters that affect their performance, Renew. Sustain. Energy Rev. 30 (2014) 337–355. doi:10.1016/j.rser.2013.10.027.

[8] E. Falletta, P. Costa, C. Della Pina, S. Lanceros-mendez, Sensors and Actuators A : Physical Development of high sensitive polyaniline based piezoresistive films by conventional and green chemistry approaches, Sensors Actuators A. Phys. 220 (2014) 13–21. doi:10.1016/j.sna.2014.09.004.

[9] D. Geethalakshmi, N. Muthukumarasamy, R. Balasundaraprabhu, Effect of dopant concentration on the properties of HCl-doped PANI thin films prepared at different temperatures, Optik (Stuttg). 125 (2014) 1307–1310. doi:10.1016/j.ijleo.2013.08.014.

[10] S. Xu, J. Yan, Z. Feng, S. Qiu, F. Shao, M. Li, M. Yu, H. Qiu, Electrical transport properties of Ni80Fe20/HCl-PANI composites, Thin Solid Films. 608 (2016) 44–49. doi:10.1016/j.tsf.2016.04.009.

[11] X.X. Gong, G.T. Fei, W.B. Fu, M. Fang, X.D. Gao, B.N. Zhong, L. De Zhang,

Flexible strain sensor with high performance based on PANI/PDMS films, Org. Electron. Physics, Mater. Appl. 47 (2017) 51–56. doi:10.1016/j.orgel.2017.05.001.

[12] S. Ray, A.J. Easteal, R.P. Cooney, N.R. Edmonds, Structure and properties of melt-processed PVDF/PMMA/polyaniline blends, Mater. Chem. Phys. 113 (2009) 829–838. doi:10.1016/j.matchemphys.2008.08.034.

[13] T. Del Castillo-Castro, M.M. Castillo-Ortega, P.J. Herrera-Franco, Electrical, mechanical and piezo-resistive behavior of a polyaniline/poly(n-butyl methacrylate) composite, Compos. Part A Appl. Sci. Manuf. 40 (2009) 1573–1579. doi:10.1016/j.compositesa.2009.07.001.

[14] J. Teixeira, L. Horta-Romarís, M.J. Abad, P. Costa, S. Lanceros-Méndez, Piezoresistive response of extruded polyaniline/(styrene-butadiene-styrene) polymer blends for force and deformation sensors, Mater. Des. 141 (2018) 1–8. doi:10.1016/j.matdes.2017.12.011.

[15] G.M.O. Barra, R.R. Matins, K.A. Kafer, R. Paniago, C.T. Vasques, A.T.N. Pires, Thermoplastic elastomer/polyaniline blends: Evaluation of mechanical and electromechanical properties, Polym. Test. 27 (2008) 886–892. doi:10.1016/j.polymertesting.2008.07.004.

[16] Z.S. Levin, C. Robert, J.F. Feller, M. Castro, J.C. Grunlan, Flexible latex—polyaniline segregated network composite coating capable of measuring large strain on epoxy, Smart Mater. Struct. 22 (2013) 15008. doi:10.1088/0964-1726/22/1/015008.

[17] C. Micolini, F. Holness, J. Johnson, A. Price, Assessment of Embedded Conjugated Polymer Sensor Arrays for Potential Load Transmission Measurement in Orthopaedic Implants, Sensors. 17 (2017) 2768. doi:10.3390/s17122768.

[18] Y. Du, S.Z. Shen, K. Cai, P.S. Casey, Research progress on polymer-inorganic thermoelectric nanocomposite materials, Prog. Polym. Sci. 37 (2012) 820–841. doi:10.1016/j.progpolymsci.2011.11.003.

[19] M. Culebras, C.M. Gómez, A. Cantarero, Review on polymers for thermoelectric applications, Materials (Basel). 6 (2014) 6701–6732. doi:10.3390/ma7096701.

[20] A. Dey, O.P. Bajpai, A.K. Sikder, S. Chattopadhyay, M.A. Shafeeuulla Khan, Recent advances in CNT/graphene based thermoelectric polymer nanocomposite: A proficient move towards waste energy harvesting, Renew. Sustain. Energy

Rev. 53 (2016) 653–671. doi:10.1016/j.rser.2015.09.004.

[21] B. Guo, Z. Tang, L. Zhang, Transport performance in novel elastomer nanocomposites: Mechanism, design and control, Prog. Polym. Sci. 61 (2016) 29–66. doi:10.1016/j.progpolymsci.2016.06.001.

[22] E.E. Tkalya, M. Ghislandi, G. de With, C.E. Koning, The use of surfactants for dispersing carbon nanotubes and graphene to make conductive nanocomposites, Curr. Opin. Colloid Interface Sci. 17 (2012) 225–232. doi:10.1016/j.cocis.2012.03.001.

[23] H. Pang, L. Xu, D.X. Yan, Z.M. Li, Conductive polymer composites with segregated structures, Prog. Polym. Sci. 39 (2014) 1908–1933. doi:10.1016/j.progpolymsci.2014.07.007.

[24] H. Park, T. Kim, J. Huh, M. Kang, J.E. Lee, H. Yoon, P.E.T. Al, Anisotropic Growth Control of Polyaniline Nanostructures and Their Morphology-Dependent Electrochemical Characteristics, (2012) 7624–7633.

[25] M. Wojdyr, Fityk: a general-purpose peak fitting program, J. Appl. Crystallogr. 43 (2010) 1126–1128.

[26] J.P. Pouget, M.E. Jozefowicz, A.J. Epstein, X. Tang, A.G. MacDiarmid, X-ray structure of polyaniline, Macromolecules. 24 (1991) 779–789. doi:10.1021/ma00003a022.

[27] UNE-EN ISO 11357-4, Plásticos. Calorimetría diferencial de barrido (DSC). Parte 4: Determinación de la capacidad térmica específica, (2014).

[28] P. Costa, J. Nunes-Pereira, J. Oliveira, J. Silva, J.A. Moreira, S.A.C. Carabineiro, J.G. Buijnsters, S. Lanceros-Mendez, High-performance graphene-based carbon nanofiller/polymer composites for piezoresistive sensor applications, Compos. Sci. Technol. 153 (2017) 241–252. doi:10.1016/j.compscitech.2017.11.001.

[29] B.F. Gonçalves, J. Oliveira, P. Costa, V. Correia, P. Martins, G. Botelho, S. Lanceros-Mendez, Development of water-based printable piezoresistive sensors for large strain applications, Compos. Part B Eng. 112 (2017) 344–352. doi:10.1016/j.compositesb.2016.12.047.

[30] L. Horta-Romarís, M.-J. Abad, M.V. González-Rodríguez, A. Lasagabáster, P. Costa, S. Lanceros-Mendez, Cyclic temperature dependence of electrical conductivity in polyanilines as a function of the dopant and synthesis method, Mater. Des. 114 (2016) 288–296. doi:10.1016/j.matdes.2016.11.021.

[31] A.A. Patel, J.R. Feng, M.A. Winnik, G.J. Vancso, C.B.D. Mcbain,

Characterization of latex blend films by atomic force microscopy, Polymer (Guildf). 37 (1996) 5577–5582. http://bibliocheveu/connaissances/cheveu/bibliocheveu/Surfaces/2589_Patel AA_1996.pdf.

[32] M. Füllbrandt, P.J. Purohit, A. Schönhals, Combined FTIR and Dielectric Investigation of Poly(vinyl acetate) Adsorbed on Silica Particles, Macromolecules. 46 (2013) 4626–4632. doi:10.1021/ma400461p.

[33] M.S. Dopico-García, A. Ares, A. Lasagabáster-Latorre, X. García, L. Arboleda, M.J. Abad, Extruded polyaniline/EVA blends: Enhancing electrical conductivity using gallate compatibilizers, Synth. Met. 189 (2014) 193–202. doi:10.1016/j.synthmet.2014.01.009.

[34] L. Horta-Romar??s, M.J. Abad, M.V. Gonz??lez-Rodr??guez, A. Lasagab??ster, P. Costa, S. Lanceros-M??ndez, Cyclic temperature dependence of electrical conductivity in polyanilines as a function of the dopant and synthesis method, Mater. Des. 114 (2017) 288–296. doi:10.1016/j.matdes.2016.11.021.

[35] J.D. Crawford, Introduction to bifurcation theory, Rev. Mod. Phys. 63 (1991) 991–1037. doi:10.1103/RevModPhys.63.991.

[36] M. Weber, M.R. Kamal, Estimation of the volume resistivity of electrically conductive composites, Polym. Compos. 18 (1997) 711–725. doi:10.1002/pc.10324.

[37] P. Beadle, S.P. Armes, S. Gottesfeld, C. Mombourquette, R. Houlton, W.D. Andrews, S.F. Agnew, Electrically Conductive Polyaniline-Copolymer Latex Composites, Macromolecules. 25 (1992) 2526–2530. doi:10.1021/ma00035a035.

[38] X. Wu, C. Lu, H. Xu, X. Zhang, Z. Zhou, Xiaodong Wu, Canhui Lu, Haoyu Xu, Xinxing Zhang, * and Zehang Zhou, Appl. Mater. Interfaces. 6 (2014) 21078–21085.

[39] C. Yu, Y.S. Kim, D. Kim, J.C. Grunlan, Thermoelectric behavior of segregated-network polymer nanocomposites, Nano Lett. 8 (2008) 4428–4432. doi:10.1021/nl802345s.

[40] W. Meixiang, Wan; Lijuan, Liu; Jun, Electrical and Mechanical Properties of Polyanailine Films - Effect of Neutral Salts Added During Polymerization, Chinese J. Polym. Sci. 16 (1998).

[41] H. Valentová, J. Stejskal, Mechanical properties of polyaniline, Synth. Met. 160 (2010) 832–834. doi:10.1016/j.synthmet.2010.01.007.

[42] B. Rimez, H. Rahier, G. Van Assche, T. Artoos, B. Van Mele, The thermal degradation of poly(vinyl acetate) and poly(ethylene-co-vinyl acetate), Part II: Modelling the degradation kinetics, Polym. Degrad. Stab. 93 (2008) 1222–1230. doi:10.1016/j.polymdegradstab.2008.01.021.

[43] Elisabeth E. C. Monteiro and Clelio Thaumaturgo, SURFACE PHENOMENA AND POLYMER MISCIBILITY OF PVC/EVA BLENDS, Compos. Sci. Technol. 57 (1997) 1159–1165.

[44] O. Kanoun, C. Müller, A. Benchirouf, A. Sanli, T. Dinh, A. Al-Hamry, L. Bu, C. Gerlach, A. Bouhamed, Flexible Carbon Nanotube Films for High Performance Strain Sensors, Sensors. 14 (2014) 10042–10071. doi:10.3390/s140610042.

[45] A. Ferrreira, J.G. Rocha, A. Ansón-Casaos, M.T. Martínez, F. Vaz, S. Lanceros-Mendez, Electromechanical performance of poly(vinylidene fluoride)/carbon nanotube composites for strain sensor applications, Sensors Actuators, A Phys. 178 (2012) 10–16. doi:10.1016/j.sna.2012.01.041.

[46] T. Chen, C. Dong, X. Li, J. Gao, Thermal degradation mechanism of dodecylbenzene sulfonic acid-hydrochloric acid co-doped polyaniline, Polym. Degrad. Stab. 94 (2009) 1788–1794. doi:10.1016/j.polymdegradstab.2009.06.011.

[47] P. Costa, C. Silvia, J.C. Viana, S. Lanceros Mendez, Extruded thermoplastic elastomers styrene-butadiene-styrene/carbon nanotubes composites for strain sensor applications, Compos. Part B Eng. 57 (2014) 242–249. doi:10.1016/j.compositesb.2013.10.006.